Received <day> <Month>, <year>; | Revised <day> <Month>, <year>; | Accepted <day> <Month>, <year>

DOI: xxx/xxxx

ARTICLE TYPE

Hybrid TLM-CTLM Test Structure for Determining Specific Contact Resistivity of Ohmic Contacts

Pan Yue[1] | Thanh Pham Chi[2] | Anthony Holland[1]

[1]School of Engineering, RMIT University, Victoria, Australia.
[2]School of Science, Engineering and Technology, RMIT University Vietnam, HoChiMinh city, Vietnam.

Correspondence
*Thanh Pham Chi, 702 Nguyen Van Linh Blvd., HoChiMinh city, Vietnam. Email: s3251886@rmit.edu.vn or thanh.pham@rmit.edu.vn

Abstract

Various test structures can be used to determine the specific contact resistivity of ohmic contacts. The transmission line model test structure and circular transmission line model test structure are the most commonly used. The analytical expressions of the former are straightforward and effectively describe the electrical behavior of a contact, while the concentric geometry of the latter eliminates complications during fabrication. In this paper, we present a hybrid test structure that combines the advantages of the transmission line and the circular transmission line models. The analytical expressions of the new structure are presented, and its finite-element modeling is undertaken. The effect of contact geometry on this test structure is also discussed. Using the presented test structure, determining contact parameters does not require any error corrections.

KEYWORDS:
test structure; ohmic contact; TLM; CTLM; specific contact resistivity

DEFINTIION

α	Attenuation constant, the inverse of the transfer length (L_T) in the transmission line model (in per centimeter), $\alpha^2 = R_{SH}/\rho_C$
d	The gap width between the central contact and the outer contact (in micrometers).
$\triangle$	An experimentally determined factor for extracting ρ_C (in per ohms).
I	Current through the contacts (in milliamperes).
L	The width of the contacts in the transmission line model portion of the hybrid test structure (in micrometers).
L_T	Transfer length (in micrometers).
ϕ	An experimentally determined factor for extracting ρ_C (no unit).
R_A	The resistance due to the circular transmission line model portion of the hybrid test structure (in ohms).
R_B	The resistance due to the transmission line model portion of the hybrid test structure (in ohms).
R_{C0}	Central dot contact resistance in the circular transmission line model portion of the hybrid test structure (in ohms).
R_{C1}	Outer electrode contact resistance in the circular transmission line model portion of the hybrid test structure (in ohms).
ρ_C	Specific contact resistivity (in ohms square centimeter).

R_P	The resistance due to the semiconductor layer, which surrounds the central dot electrode in the circular transmission line model portion of the hybrid test structure (in ohms).
R_{SH}	Sheet resistance of the semiconductor layer (in ohm per square).
R_T	Measured resistance between the central and outer electrodes (in ohms).
V	Measured voltage drop, central dot electrode to outer electrode (in millivolts).
W	The length of the contacts in the transmission line model portion of the hybrid test structure (in micrometers).

1 | INTRODUCTION

Metal-to-semiconductor (M-S) contacts have been studied since 1874[1] because of their importance in solid-state physics[2]. These contacts are used in various applications, such as Schottky contacts in the anode and cathode in p-n diodes[3], and ohmic electrical contacts for the source and drain electrodes in metal oxide semiconductor field-effect transistors (MOSFETs). As transistor dimensions shrink in new technology nodes, contact resistance (R_C) significantly affects the switching speed and power consumption of transistors[4,5]. For instance, R_C accounts for 25% of the transistor's on-state resistance in 7-nm and 5-nm CMOS technology nodes[6]. With recent advances in FET technology, such as the transition from the long-lasting planar FET structure to FinFETs, Gate-All-Around FETs (GAAFETs), and Multi-Bridge-Channel FETs (MBCFETs)[7,8,9], it is essential that electrical contacts keep pace with the new technologies. Therefore, studying, and characterising ohmic contacts in modern semiconductor devices becomes crucial.

Specific contact resistivity (SCR, symbol as ρ_C) is an extremely important parameter for quantifying an ohmic contact. The International Roadmap for Devices and Systems (IRDS), an authoritative source for guiding industry-relevant research, stated that for technology nodes below 5 nm, CMOS technology requires SCR to be below $1x10^{-9}$ $\Omega.cm^2$[4]. SCR characterisation typically involves using ohmic contact test structures[10,11,12]. Yu et al.[3] presented a family of TLM-based test structures, comparing them in terms of the range of ρ_C they can measure and the complexity of their fabrication processes. Among them, the Transmission Line Model (TLM), also referred to as Linear TLM, is regarded as the most widely used test structure for characterising planar ohmic contacts[13], inspiring different generations of linear TLM-based structures over the years. Recent linear structures include the refined TLM[14], the ladder TLM[15], and refined ladder TLM[16], introducing new analytical expressions and test structure changes that enable the measurement of ultra-low values of SCR.

The conventional TLM has relatively simple analytical equations for determining SCR. However, it requires mesa etch to confine the active region in the semiconductor[12] . This mesa etch can be eliminated using the Circular Transmission Line Model (CLTM), but the analytical expression for the CTLM is relatively complicated and it is difficult to keep an equipotential at the middle ring contact in the CTLM[17]. Circular TLM and its variants, such as the two-contact circular test structure[18], multiring CTLM[19], and coaxial circular test structure[20], offer a more efficient alternative to the rectangular patterns of linear TLM test structures.

Finite element modelling (FEM) is a numerical technique used in computer simulation for engineering analysis and problem-solving[21]. FEM has been employed in semiconductor device simulation since the 1980s[22], offering benefits such as representing complex geometries, including dissimilar material properties, and capturing local effects[23]. Computations at each node are assembled to model the entire device, allowing for precise analysis[24]. Synopsys Sentaurus TCAD[25] has been widely used for studying scaling effects on FinFETs and GAAFETs at the 3-nm node and beyond[8], device failure analysis of the fabrication process of 3D devices such as modern FinFETs[26], and radiation damage effects on high voltage CMOS monolithic active pixel sensors[27].

Specifically relevant to this paper's focus on ohmic contact test structures, Sentaurus TCAD has been used to model contact resistance in FinFETs[28], planar contacts in TLM test structures[29] and newly proposed ohmic contact test structures such as R-LTLM[16] and LTM[15]. Other FEM tools have been employed in related studies, such as using COMSOL Multiphysics[30] to model nanoscale electrical junctions and electrical contacts in metal-insulator-metal (MIM) junctions[31], and ANSYS™[32] to investigate the thermoelectrical behaviour of ohmic microcontacts[21]. For CTLM test structures, MSC Nastran and Patran[33] was used for modelling and characterising SCR for ohmic contacts using two-contact circular test structures[17], and for determining specific contact resistivity of contacts to bulk semiconductors using two-contact circular test structures[34].

In this paper, a new hybrid test structure is proposed that combines the advantages of the TLM and CTLM. The combined model inherits simple analytical equations from the TLM, while its CTLM-like geometry simplifies the fabrication process. The latter is an attractive feature suitable for materials that are difficult to etch, such as SiC. The paper is organised as follows:

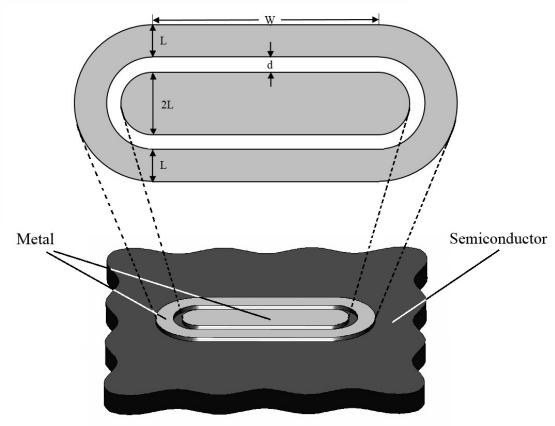

FIGURE 1 Isometric view of the hybrid TLM-CTLM test structure. Total resistance R_T is measured between the central electrode and the outer electrode.

Section II introduces the newly proposed test structure and its analytical expressions for determining specific contact resistivity (SCR). Section III describes the finite-element model used to compare with typical SiC metal-semiconductor (M-S) parameters to verify the structure. Section IV presents the results and discusses the findings from the analysis, including the effect of contact geometry on the structure. Finally, Section V draws conclusions and summarises the key findings.

2 | HYBRID TLM-CTLM TWO-CONTACT TEST STRUCTURE

The hybrid TLM-CTLM test structure consists of two half-CTLM patterns and a TLM pattern between them. As shown in Figure 1, the width and the length of the central TLM rectangular contact are W and $2L$, respectively. The length of the TLM rectangular contacts for the outer contact is L. The gap between the central contact and the outer contact is d. Figure 2 shows the resistance representation of the test structure in Figure 1. When current I is forced between the two metal contacts, the total resistance R_T can be determined by measuring the voltage between the electrodes V_T, using Equation (1).

$$R_T = \frac{V}{I} \tag{1}$$

R_T consists of resistance R_A due to the CTLM portion and resistance R_B due to the TLM portion. Since R_A and R_B are in parallel R_T can be written as in Equation (2).

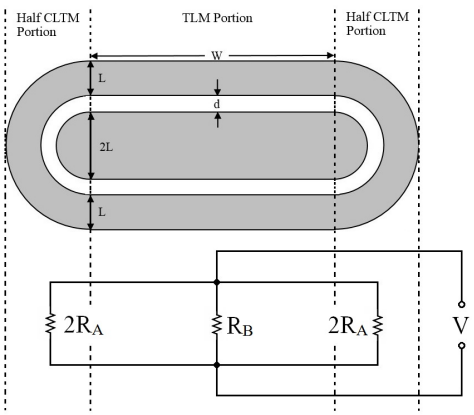

FIGURE 2 Schematic of the hybrid TLM-CTLM test structure. Total resistance R_T consists of R_A and R_B.

$$R_T = \frac{1}{\frac{1}{2R_A} + \frac{1}{R_B} + \frac{1}{2R_A}} = \frac{R_A.R_B}{R_A + R_B} \tag{2}$$

The components of the analytical model for R_T are determined as follows.

2.1 | Resistance R_A due to the CTLM Portions

The two half-CTLM patterns can be considered as a whole CTLM test structure. As reported by Yue et at.[18], R_A consists of the central dot contact resistance R_{C0}, the resistance due to the semiconductor ring R_P and the outer electrode resistance R_{C1} as in Equation (3)

$$R_A = R_{C0} + R_P + R_{C1} \tag{3}$$

2.2 | Resistance R_A due to the TLM Portion

The resistance due to the TLM portion in the middle of the proposed test structure can be considered as two equal resistances which are the total resistances between two rectangular electrodes with the same size (L x W) in parallel as in Equation (4)

$$R_B = \frac{1}{2}(\frac{R_{SH}.d}{W} + 2R_C) \tag{4}$$

where R_C is the contact resistance under each rectangular contact described in Equation (5)

$$R_C = \frac{\sqrt{R_{SH}.\rho_C}}{W}.coth(\frac{L}{L_T}) \tag{5}$$

L_T is the transfer length, which is defined in Equation (6)

$$L_T = \frac{1}{\alpha} = \sqrt{\frac{\rho_C}{R_{SH}}} \tag{6}$$

when L_T is shorter than $0.5L$, $\coth(L/L_T) \rightarrow 1$, hence, Equation (4) can be reduced to Equation (7)

$$R_B = \frac{R_{SH}}{2W}(d + 2L_T) \tag{7}$$

3 | FINITE-ELEMENT MODELING

Finite element modelling (FEM) can be used to accurately model the electrical behaviour of ohmic contacts between a metal and a semiconductor. Forming a model requires information on contact structure geometry, the conductivity of each layer in the structure, and ρ_C of each interface in the structure. In this work, MSC Nastran and Patran software are used to model the hybrid TLM-CTLM test structure. MSC Nastran is a finite element program developed by NASA for heat transfer analysis, mechanical analysis while MSC Patran is used for creating models and meshing[33]. However, voltage distribution in materials can also be obtained by using MSC Nastran because the equation for electrical current transfer (Ohms's Law) is analogous to that of the heat transfer (Fourier's Law).

A hybrid TLM-CTLM test structure with L, d and W values of 50, 25 and 300 μm respectively, is constructed in MSC Patran. In order to reduce the time taken for analysis, only a quarter of the whole structure is modeled (see Figure 3). Considering the symmetry in the structure, this quarter portion is representative of the whole structure. Each metal contact is assumed to be an equipotential, and this implies zero sheet resistance for the metal layer. The thickness of the semiconductor layer was 0.3 μm. The equipotential of the outer electrode surface is set to zero, and the current is input at the central electrode. Figure 3 shows the equipotentials and structure geometry of an example model for analysis where R_{SH}= 3000 Ω/ □ and ρ_C = 1 x 10^{-4} Ω.cm^2.

Next, the results from the FEM model will be extracted and compared against ones calculated using the analytical equations from the previous section to evaluate the accuracy of the test structure.

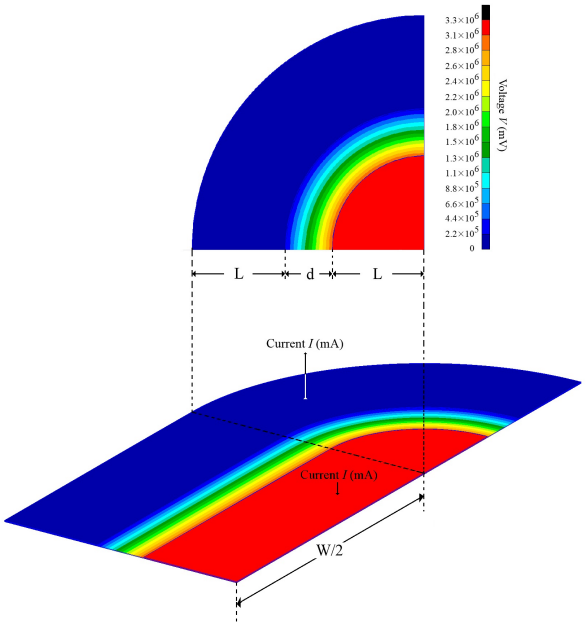

FIGURE 3 Equipotentials (in millivolts) in the semiconductor layer for the hybrid TLM-CTLM test structure FEM (a quarter of the test structure is presented).

4 | RESULTS AND DISCUSSION

4.1 | Analysing Resistance Component Plots

The first analysis varies the dimensions of the test structure and compares the total resistance plots. For instance, W is varied from 5 to 500 μm, while L and d are fixed at 50 and 25 μm respectively. For each variation, R_T from the FEM model is determined using the equipotential difference between the central electrode and the outer electrode, and the input current using Ohm's Law. This is then compared against R_T calculated using the analytical expressions. For each width value, one can also determine the corresponding transfer length value L_T. Figure 4 summarises the results and shows that the analytical and FEM results are in good agreement with increasing W.

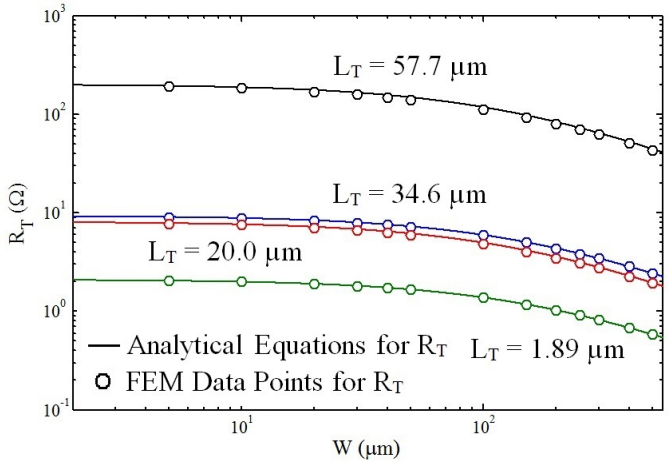

FIGURE 4 Comparison of R_T versus W plots for different test structure dimensions, with W ranging from 5 to 500 μm, $L = 50$, $d = 25$ μm. Corresponding L_T values are 1.89, 20.0, 34.6 and 57.7 μm.

4.2 | Methodology to Extract Specific Contact Resistivity

This section details the methodology to extract SCR value using the proposed test structure. The complete test pattern set is shown in Fig. 5. The set consists of four hybrid TLM-CTLM patterns with different values of d and W, while L is kept the same.

The resistances for the patterns in Figure 5(a) and Figure 5(b) are denoted as R_{T1} and R_{T2} accordingly. These can be represented using Equation (8) and (9). R_{Ax} and R_{Bx}, where x = 1,2, are component resistance due to the CTLM and TLM portions, as described in Section 2.

$$\frac{1}{R_{T1}} = \frac{1}{R_{A1}} + \frac{1}{R_{B1}} \tag{8}$$

$$\frac{1}{R_{T2}} = \frac{1}{R_{A1}} + \frac{1}{R_{B2}} \tag{9}$$

Substituting Equations (4) and (5), to (8) and (9), we can yield Equation (10)

$$\frac{1}{R_{T1}} - \frac{1}{R_{T2}} = \frac{1}{R_{B1}} - \frac{1}{R_{B2}} = \frac{2(W_1 - W_2)}{R_{SH}[d_1 + 2L_T.coth(L/L_T)]} \tag{10}$$

Similarly, considering total resistance for two patterns in Figure 5(c) and Figure 5(d), we have them expressed as in Equation (11) and (12)

$$\frac{1}{R'_{T1}} = \frac{1}{R'_{A1}} + \frac{1}{R'_{B1}} \tag{11}$$

$$\frac{1}{R'_{T2}} = \frac{1}{R'_{A1}} + \frac{1}{R'_{B2}} \tag{12}$$

Substituting Equations (4) and (5), to (11) and (12), we can yield Equation (13)

$$\frac{1}{R'_{T1}} - \frac{1}{R'_{T2}} = \frac{1}{R'_{B1}} - \frac{1}{R'_{B2}} = \frac{2(W_1 - W_2)}{R_{SH}[d_2 + 2L_T.coth(L/L_T)]} \tag{13}$$

R_{SH} can be determined using Equation (14) by eliminating L_T in Equations (10) and (13)

$$R_{SH} = \frac{d_2 - d_1}{2(W_2 - W_1)}.\triangle \tag{14}$$

where $\triangle$ is a factor that can be experimentally determined from measured resistance as in Equation (15)

$$\triangle = \frac{(R_{T2} - R_{T1}).(R'_{T2} - R'_{T1})}{R_{T1}R_{T2}.(R'_{T2} - R'_{T1}) - R'_{T1}R'_{T2}.(R_{T2} - R_{T1})} \tag{15}$$

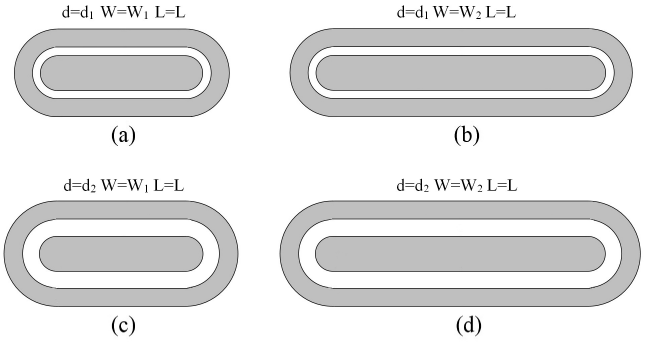

FIGURE 5 Complete test pattern set used to extract R_{SH} and ρ_C using the hybrid TLM-CTLM test structure.

Eliminating R_{SH} in Equations (10) and (13), L_T can be found using Equation (16)

$$\frac{d_2 + 2L_T.coth(L/L_T)}{d_1 + 2L_T.coth(L/L_T)} = \frac{R_{T2} - R_{T1}}{R_{T1}.R_{T2}} \cdot \frac{R'_{T1}.R'_{T2}}{R'_{T2} - R'_{T1}} \tag{16}$$

If L is greater than $2L_T$, coth(L/L_T) → 1, Equation (16) can be reduced to Equation (17)

$$L_T = \frac{d_2 - \phi.d_1}{2\phi - 2} \tag{17}$$

where ϕ can also be experimental determined using Equation (18)

$$\phi = \frac{R_{T2} - R_{T1}}{R_{T1}.R_{T2}} \cdot \frac{R'_{T1}.R'_{T2}}{R'_{T2} - R'_{T1}} \tag{18}$$

With known R_{SH} and L_T, ρ_C can be found using Equation (6) using (6).

4.3 | The Effect of Contact Geometry

The geometry of the proposed hybrid structure (refer to Figure 2) shows that the inner perimeter of the outer contact is always longer than the perimeter of the central contact. When a current is forced between the two contacts, some of it will flow from the TLM portion to the CTLM portion at the place where they meet. This is because the CTLM portion has a lower current density than the TLM portion at the fringe. This fringe effect becomes significant when the transfer length becomes relatively big with respect to d, W, and L. It will lead to a significant error when extracting ρ_C using the method presented in this paper. Figure 6 illustrates such a scenario for a structure with $d = 25$, $L = 50$, and $W = 300$ μm, $R_{SH} = 30$ Ω/□, and $\rho_C = 4.8$ x 10^{-4} Ω.cm^2. The transfer length is calculated as $L_T = 40$ μm, which is considered large with respect to the test structure dimensions. It can be seen that the voltage contour is not flowing parallel in the area between the central and outer contacts.

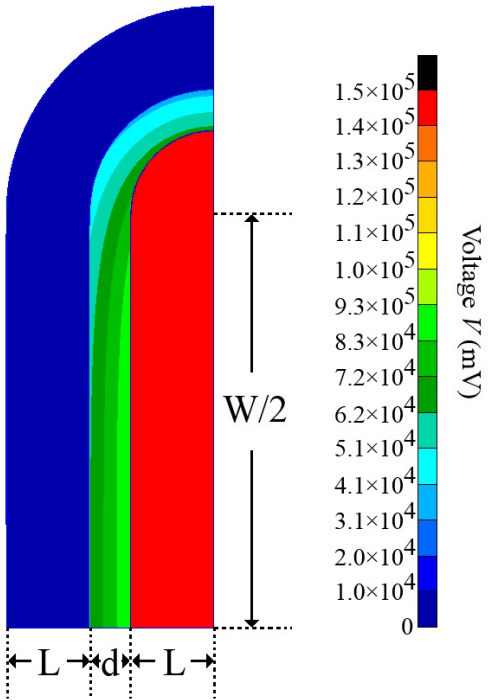

FIGURE 6 Fringe effect shown in the voltage contour of the hybrid TLM-CTLM test structure FEM model.

Analysing Equations (10), (13), and the voltage contour, it can be seen that once W exceeds a certain W_{min} value, the voltage contours in the middle region become perfectly parallel. In other words, current can then flow straight to the outer contact perfectly, and this fringe effect can be eliminated. To find this W_{min}, a number of test structure geometries are constructed and modeled. Specifically, all variations have fixed d = 25 and L = 50 μm. The transfer length L_T is varied from 0.1 to 50 μm (this range can cover most of the typical values of L_T for actual SiC ohmic contacts). W is varied up to 1000 μm.

After intensive analysis of these test structure geometry variations, the results show that with fixed d and L, the fringe effect can be eliminated if $W \geq W_{min} = 8L_T$. For instance, for $0 < L_T < 50$ μm, the fringe effect can be eliminated when $W > 400$ μm. Only then can the analytical equations presented in the previous section be applied to determine ρ_C accurately.

5 | CONCLUSION

This paper introduces a hybrid TLM-CTLM test structure that combines the analytical simplicity of TLM with the fabrication advantages of CTLM. FEM demonstrates its accuracy in determining specific contact resistivity without error corrections. A study on its geometry shows that the structure's width must be at least eight times the transfer length. This condition ensures the elimination of fringe effects and the validity of the analytical equations. Future work includes manufacturing such structures for specific ohmic contact technology such as SiC and applying its analytical expressions and methods to extract ρ_C for such contacts.

References

1. Braun F. Ueber die stromleitung durch schwefelmetalle. *Annalen der Physik* 1875; 229(12): 556-563.
2. Sze SM, Li Y, Ng KK. *Physics of semiconductor devices*. John wiley 'I&' sons . 2021.
3. Sharma B. *Metal-semiconductor Schottky barrier junctions and their applications*. Springer New York, NY . 1984
4. IEEE . The International Roadmap for Devices and Systems: 2022 Edition - Executive Summary. 2022.
5. Yeric G. Moore's law at 50: Are we planning for retirement?. In: : 1.1.1-1.1.8
6. Yu H, Schaekers M, Everaert JL, Horiguchi N, De Meyer K, Collaert N. A snapshot review on metal–semiconductor contact exploration for 7-nm CMOS technology and beyond. *MRS Advances* 2022; 7(36): 1369-1379. doi: 10.1557/s43580-022-00404-1
7. Das RR, Rajalekshmi TR, James A. FinFET to GAA MBCFET: A Review and Insights. *IEEE Access* 2024; 12: 50556-50577. doi: 10.1109/ACCESS.2024.3384428
8. Das UK, Bhattacharyya TK. Opportunities in Device Scaling for 3-nm Node and Beyond: FinFET Versus GAA-FET Versus UFET. *IEEE Transactions on Electron Devices* 2020; 67(6): 2633-2638. doi: 10.1109/TED.2020.2987139
9. Jeong J, Lee SH, Masuoka SA, et al. World's First GAA 3nm Foundry platform Technology (SF3) with Novel Multi-Bridge-Channel-FET (MBCFET^{TM}) Process. In: : 1-2
10. Shockley W, Goetzberger A, Scarlett R. Research and investigation of inverse epitaxial UHF power transistors. *Rep. No Al-TOR-64-207 Air Force At. Lab. Wright-Patterson Air Force Base Ohio* 1964.
11. Berger H. Models for contacts to planar devices. *Solid-State Electronics* 1972; 15(2): 145-158. doi: https://doi.org/10.1016/0038-1101(72)90048-2
12. Reeves GK. Specific contact resistance using a circular transmission line model. *Solid-State Electronics* 1980; 23(5): 487-490. doi: https://doi.org/10.1016/0038-1101(80)90086-6
13. Sun Z, Huang H, Liu Y, et al. A Novel Analytical Model for Ohmic Contacts to Planar Devices: Theoretical Design and Experimental Verification. *IEEE Transactions on Electron Devices* 2021; 68(1): 299-306. doi: 10.1109/TED.2020.3037880

14. Dormaier R, Mohney SE. Factors controlling the resistance of Ohmic contacts to n-InGaAs. *Journal of Vacuum Science 'I&' Technology B* 2012; 30(3): 031209. doi: 10.1116/1.4705730doi: 10.1116/1.4705730

15. Wu Y, Xu H, Gong X, Yeo YC. A Ladder Transmission Line Model for the Extraction of Ultralow Specific Contact Resistivity—Part I: Theoretical Design and Simulation Study. *IEEE Transactions on Electron Devices* 2020; 67(7): 2682-2689. doi: 10.1109/TED.2020.2992988

16. Sun X, Luo J, Liu Y, et al. A Refined Ladder Transmission Line Model for the Extraction of Significantly Low Specific Contact Resistivity. *IEEE Transactions on Electron Devices* 2023; 70(1): 209-214. doi: 10.1109/TED.2022.3221380

17. Pan Y, Reeves GK, Leech PW, Holland AS. Analytical and Finite-Element Modeling of a Two-Contact Circular Test Structure for Specific Contact Resistivity. *IEEE Transactions on Electron Devices* 2013; 60(3): 1202-1207. doi: 10.1109/TED.2013.2242076

18. Pan Y, Reeves GK, Leech PW, Tanner P, Holland AS. Two-contact Circular Test Structure for Determining Specific Contact Resistivity. *MRS Online Proceedings Library* 2013; 1553(1): 313. doi: 10.1557/opl.2013.864

19. Yu H, Schaekers M, Schram T, et al. Multiring Circular Transmission Line Model for Ultralow Contact Resistivity Extraction. *IEEE Electron Device Letters* 2015; 36(6): 600-602. doi: 10.1109/LED.2015.2425792

20. Miyazawa N, Usami N, Wang H, et al. Coaxial Circular Test Structure Applicable to both Ohmic and Schottky Characteristics for ZnO/Si Heterojunctions Assessment. In: : 1-4

21. Liu H, Leray D, Pons P, Colin S. Finite element multi-physics modeling for ohmic contact of microswitches. In: : 1-8

22. Buturla EM, Cottrell PE, Grossman BM, Salsburg KA. Finite-Element Analysis of Semiconductor Devices: The FIELDAY Program. *IBM Journal of Research and Development* 1981; 25(4): 218-231. doi: 10.1147/rd.254.0218

23. Jerome JW. *Analysis of charge transport: a mathematical study of semiconductor devices*. Springer Science 'I&' Business Media . 2012.

24. Xeni N, Ghannam R, Adamu-Lema F, Badami O, Georgiev V, Asenov A. The Use of Tcad Simulations in Semiconductor Devices Teaching. In: : 1-4

25. Synopsys . Sentaurus TCAD J-2019. 2019.

26. Lim SY, Ghosh J, Thean A. Innovative use of TCAD Process Simulation for Device Failure Analysis. In: : 1-4

27. Bui TA, Reeves GK, Leech PW, Holland AW, Taylor G. TCAD simulation of a single Monolithic Active Pixel Sensors based on High Voltage CMOS technology. *MRS Advances* 2018; 3(51): 3053-3059. doi: 10.1557/adv.2018.417

28. Feng P, Kim J, Cho J, et al. Contact model based on TCAD-experimental interactive algorithm. In: : 238-241

29. Pham TC, Tran HN, Partridge JG, Holland AS. Resistor-to-Schottky barrier analytical model for ohmic contact test structures. *Semiconductor Science and Technology* 2024; 39(6): 065017. doi: 10.1088/1361-6641/ad49c8

30. COMSOL . COMSOL Multiphysics. 2024.

31. Banerjee S, Zhang P. Review of recent studies on nanoscale electrical junctions and contacts: Quantum tunneling, current crowding, and interface engineering. *Journal of Vacuum Science 'I&' Technology A* 2022; 40(3): 030802. doi: 10.1116/6.0001724

32. Ansys . Ansys | Engineering Simulation Software. 2024.

33. Software M. MSC Nastran and Patran. 2024.

34. Pan Y, Collins AM, Holland AS. Determining specific contact resistivity of contacts to bulk semiconductor using a two-contact circular test structure. In: : 257-260